Destabilization of the Tumor-Inducing Plasmid from an Octopine-Type *Agrobacterium tumefaciens* Lineage Drives a Large Deletion in the Co-Resident At Megaplasmid

Ian S. Barton[a], Thomas G. Platt[b], Douglas B. Rusch[c] and Clay Fuqua[a*]

[a]Department of Biology
Indiana University
Bloomington, Indiana, USA

[b]Division of Biology
Kansas State University
Manhattan, KS 66506

[c]Center for Genomics and Bioinformatics
Indiana University
Bloomington, IN 47405

Running Head: Megaplasmid deletion in *Agrobacterium*

*Address for correspondence: Clay Fuqua, Dept. Biol., 1001 E. 3rd St., Jordan Hall 142, Indiana Univ., Bloomington, IN 47405-1847. Tel: 812-856-6005, FAX: 812-855-6705,
E-mail: cfuqua@indiana.edu

Word Count: 7776 (not including abstract, references and figures legends)

Figures: 6; Tables 1, Supplementary Figures 7, Supp. Tables, 4

ABSTRACT

Bacteria with multi-replicon genome organizations, including members of the family *Rhizobiaceae*, often carry a variety of niche-associated functions on large plasmids. While evidence exists for cross-replicon interactions and co-evolution between replicons in many of these systems, remarkable strain-to-strain variation is observed within secondary replicons, suggesting environment-dependent fitness benefits of the accessory genome. Here, we show that curing of the tumor-inducing virulence plasmid (pTi) of an octopine-type *Agrobacterium tumefaciens* lineage drives a large deletion in the co-resident At megaplasmid (pAt). The deletion event is mediated by a repetitive IS-element, IS66, and results in a variety of environment-dependent fitness consequences, including loss of independent conjugal transfer of the plasmid. Interestingly, a similar deletion event is also found in a related *A. tumefaciens* strain, suggesting the mechanism is conserved in a subset of agrobacteria. Overall, the findings presented here uncover a novel genetic interaction between the megaplasmids of *A. tumefaciens* and provide evidence for cross-replicon interactions and co-evolution of rhizobial plasmids.

Keywords: Ti plasmid, accessory genome, plasmid curing, deletion, IS element, conjugal transfer

INTRODUCTION

Bacteria exhibit a diversity of genomic architectures and contain replicons that range from small, transient plasmids, to chromids, to secondary and primary chromosomes (diCenzo and Finan 2017). Approximately 10% of bacteria possess multi-partite genomes and it is hypothesized that this arrangement may allow increased genome size, faster growth rate, coordinated gene regulation, and adaptation to novel niches (Chain et al. 2006, diCenzo et al. 2017, diCenzo et al.

2014, Galardini et al. 2013, Slater et al. 2009). A multi-partite genome organization is likely maintained through selective pressures, but factors affecting replicon stability and their dynamic interactions are not well understood and often vary significantly between and within species.

Secondary replicons such as megaplasmids and plasmids confer a variety of niche-associated functions, such as antibiotic resistance, virulence, and symbiosis (diCenzo et al. 2017, Funnell et al. 2004). While many of these replicons are dispensable in the laboratory, they often have profound positive and negative effects on bacterial fitness in a variety of environments and can affect growth rate and competition (diCenzo et al. 2017, diCenzo et al. 2014, Finan et al. 1986, Morton et al. 2013, Morton et al. 2014), as well as numerous other phenotypes (Dougherty et al. 2014). Fitness consequences resulting from gain or loss of accessory genes and replicons are not typically measured, but likely depend on a combination of factors, including energetic demands of DNA replication, transcription and expression of specific costly functions, such as ABC transporters, as well as interactions between regulatory networks and pathways across replicons (diCenzo et al. 2017, Mauchline et al. 2014, Morton et al. 2013, Romanchuk et al. 2014).

Cross-replicon interactions and genetic regulation are both a consequence of and a limitation to stabilization of secondary replicons and have been observed in diverse bacterial species, including species of *Vibrio* (Heidelberg et al. 2000, Ramachandran et al. 2017) and *Sinorhizobium* (Barnett et al. 2004, Bobik et al. 2006, diCenzo et al. 2018, Galardini et al. 2015, Pini et al. 2015, Ronson et al. 1987). In most cases, chromosomal factors influence the regulation of secondary replicon factors, with limited regulation in the opposite direction (Agnoli et al. 2012, Barnett et al. 2004, Bobik et al. 2006, diCenzo et al. 2018, Galardini et al. 2015, Pini et al. 2015, Ronson et al. 1987), likely due to intolerance of integral pathway perturbation and the suppression of costly accessory functions required to stabilize secondary replicons. However, metabolic redundancy has been observed between rhizobial replicons (diCenzo et al.

2017, González et al. 2005), suggesting that favorable interaction and pathway integration between primary and secondary replicons occurs. However, because the majority of organisms possessing multi-partite genomes exist and transition between multiple environmental reservoirs, and are often host-associated, the extent to which cross-replicon interactions occur and their consequences are often not determined.

Here, we characterize a cross-replicon genetic interaction in an octopine-type lineage of the plant pathogen *Agrobacterium tumefaciens,* causative agent of crown gall disease on plants (Escobar et al. 2003, Van Larebeke et al. 1974, Watson et al. 1975). We observe that the process of curing the tumor-inducing (Ti) virulence plasmid drives a large deletion in the co-resident At megaplasmid of the octopine-type *A. tumefaciens* strain 15955. The deletion event is mediated by a repetitive IS-element and results in variety of environment-dependent fitness consequences. Interestingly, the deletion observed here is also present in the genome sequence of a related *A. tumefaciens* strain, suggesting that the deletion mechanism described here is common to a subset of strains in the *A. tumefaciens* genomospecies complex. Overall, the findings presented here indicate a novel and complex genetic interdigitization of these two large plasmids in *A. tumefaciens* and provides mechanistic precedent for the stabilization of and cross-replicon interactions between rhizobial plasmids.

MATERIALS AND METHODS

Reagents, media, strains, and growth conditions

All strains and plasmids used in this study are described in Table S1. Specific oligonucleotides are listed in Table S2, and all oligonucleotides used in the study are available upon request. Chemicals, antibiotics, and culture media were obtained from Fisher Scientific (Pittsburgh, PA), Sigma-Aldrich (St. Louis, MO), and GoldBio (St. Louis, MO) unless otherwise noted. Plasmid

design and verification as well as strain creation was performed as described previously (Morton et al. 2012) with specific details included in the text. Oligonucleotide primers were ordered from Integrated DNA Technologies, Coralville, IA. Single primer extension DNA sequencing was performed by ACGT, Inc., Wheeling, IL. Plasmids were introduced into *E. coli* via transformation with standard chemically competent cell preparations and into *A. tumefaciens* via electroporation or conjugation (Morton et al. 2012).

E. coli was cultured in standard LB broth with or without 1.5% (w v^{-1}) agar. Unless noted otherwise, *A. tumefaciens* strains were grown on AT minimal medium containing 0.5% (w v^{-1}) glucose and 15 mM ammonium sulfate without added $FeS0_4$ (ATGN) (Morton et al. 2012), or AT with 5% (w v^{-1}) sucrose as the sole carbon source (ATSN). When required, appropriate antibiotics were added to the medium as follows: for *E. coli*, 100 µg ml^{-1} ampicillin (Ap), 50 µg ml^{-1} gentamicin (Gm), and 50 µg ml^{-1} kanamycin (Km); and for *A. tumefaciens*, 300 µg ml^{-1} Gm, 300 µg ml^{-1} Km, and 300 µg ml^{-1} spectinomycin (Sp). For competition experiments, *A. tumefaciens* 15955 strains were grown in replete carbon (standard ATGN), limiting carbon (ATGN with 0.018% (w v^{-1}) glucose) or virulence-inducing media (Modified ATGN, replacing AT buffer with 50 µM phosphate buffer (NaH_2PO_4, Na_2HPO_4, pH 5.7) with 0.02M 2-N-[morpholino]ethanesulfonate (MES), and supplementing with 200 µM acetosyringone (Morton et al. 2012). Octopine utilization was evaluated by growing *A. tumefaciens* 15955 in AT media modified to contain octopine (3.2 mM) as the sole carbon and nitrogen source (ATO).

Precise deletion of IS66 was achieved using a previously described method (Morton et al. 2012). 500-750 bp of sequence upstream (P1 and P2) and downstream (P3 and P4) of the gene to be deleted were amplified using Phusion polymerase (New England Biolabs, Ipswich, MA). Primers P2 and P3 were designed with 5' sequences with reverse complementarity to each other's 3' proximal sequence. The complementary sequence on these two primers facilitated splicing by overlapping extension (SOE) of the two PCR products, as previously described

(Morton et al. 2012). Both flanking sequences were amplified and gel purified. The two purified products were then used as both templates and primers in a second PCR reaction, generating the final spliced product, which was ligated into pGEM-T easy (Promega) and sequenced to ensure proper splicing. The deletion construct was then excised using restriction enzymes and ligated into the suicide vector pNPTS138 cleaved with compatible restriction enzymes. The pNPTS138 plasmid confers Km resistance (Km^R) and sucrose sensitivity (Suc^S). Derivatives of pNPTS138 were introduced into *A. tumefaciens* 15955 by mating with *E. coli* S17-1/λpir carrying the appropriate construct. The ColE1 origin of pNPTS138 does not replicate in *A. tumefaciens*, necessitating single-crossover integration into the chromosome to obtain Km^R transformants. Plasmid integration was confirmed by patching onto ATGN-Km and ATSN to identify Suc^S derivatives. Excision of the integrated plasmid was then mediated by growing overnight cultures of Suc^S Km^R derivatives and plating dilutions onto ATSN. Plasmid excision was confirmed by patching Suc^R clones onto ATSN and ATGN-Km to identify Km^S derivatives. Correct deletion of the target gene was confirmed via diagnostic PCR using primers (P5/P6) flanking the deletion site.

Marked derivatives of *A. tumefaciens* 15955 were created using an approach similar to the creation of in-frame deletions (above) with minor alterations. P2 and P3 were designed to have complementarity in the form of a multiple cloning site, consisting of five restriction sites. After splicing of the PCR-amplified product into pNPTS138, the restriction sites were used to fuse in different screenable and selectable markers. Plasmid excision in Km^S derivatives of Suc^R clones were confirmed similarly, and retention of the screenable or selectable markers was verified by sequencing of PCR products.

Whole genome sequencing and bioinformatic analysis

Whole genome sequencing and assembly was performed at the Center for Genomics and Bioinformatics, Indiana University, Bloomington, IN. WT *A. tumefaciens* 15955 was sequenced and assembled *de novo* using a combination of 454 and Illumina NextSeq platforms. Sequencing of *A. tumefaciens* 15955 derivatives was performed using Illumina NextSeq 300 with 150 bp paired-end read libraries. Raw reads were trimmed using Trimmomatic ver. 0.33 (Bolger et al. 2014) and mapped to the assembled WT *A. tumefaciens* 15955 genome (above) using bowtie2 ver. 2.2.6 (Langmead et al. 2012). Mapping efficiency was >99% and concordantly mapped reads had an average insert size of ~500 bp with a normal distribution. Average coverage across the genome was at least 20X. Variation between WT *A. tumefaciens* 15955 and derivatives were determined using breseq ver. 0.24rc6 (Deatherage et al. 2014). Genome alignments and comparisons were performed with mummer and mummerplot packages of MUMmer 3.23 (Kurtz et al. 2004) and Artemis Comparison Tool (ACT) (Carver et al. 2005) visualizations of TBLASTX (https://blast.ncbi.nlm.nih.gov/Blast.cgi) data. Toxin/anti-toxin searches were performed using TAfinder (http://202.120.12.133/TAfinder/index.php) (Xie et al. 2018). Over the course of this project a group from the Academia Sinica in Taiwan deposited a complete genome sequence for the wild type *A. tumefaciens* 15955 into GenBank (Accession numbers; Bioproject PRJNA494475; Circular chrom. NZ_CP032917.1; Linear chrom. NZ_CP032918.1; pAt15955 NZ_CP032919.1; pTi15955 NZ_CP032920.1). This sequence is in near-perfect agreement with our de novo wild type sequence, and we refer to the coordinates of this deposited sequence where relevant.

Southern blotting

A ~500 bp DIG-labeled DNA probe (Sigma-Aldrich) specific to IS66 was generated with PCR (1:6 ratio dig-UTP:dTTP) using primers IBP102/IBP103 and used to probe 2.5 µg restriction

digested gDNA (*Sph*I, *Eco*RI, *Bam*HI) that had been electrophoresed on a 0.75% agarose gel (2h, 50V) and transferred to a charged nylon membrane via capillary blotting under alkaline conditions, as described previously (Fuqua et al. 1993). Restriction digests were performed at 37°C for 2 hours. Hybridizations and detection of the DIG-labeled DNA probe were performed according to manufacturer's suggestions (Sigma-Aldrich). Blots were visualized using a Bio-Rad Chemidoc.

pTi15955 curing and detection of pAt15955 segment loss

Curing of pTi15955 was performed as described by our lab previously (Morton et al. 2012) with slight modifications. The curing plasmid is similar to the pBBR1-type curing plasmids recently described (Yamamoto et al. 2018), containing two origins capable of replication in *Agrobacterium*, a Km^R cassette, and the counterselectable *sacB* marker for removal of the curing plasmid. Briefly, pSRKKm was digested with *Bam*HI (NEB) according with NEB guidelines, followed by purification using the E.Z.N.A. Cycle Pure Kit from Omega Bio-tek. The digested and purified pSRKKm backbone was then used in a three-part NEBuilder isothermal assembly reaction (New England Biolabs) with *repABC* (pTi15955) and *sacB* PCR products that were amplified from *A. tumefaciens* 15955 gDNA or purified pNPTS138, respectively, using primer pairs IBP200/IBP201 and IBP202/203 to create pIB301. NEBuilder reactions were performed as specified by the supplier using a 1:2 vector to insert ratio. pIB301 was confirmed using a combination of PCR and sequencing.

pIB301 was introduced into *A. tumefaciens* 15955 backgrounds via conjugation from *E. coli* S17-1/λpir donor and *A. tumefaciens* 15955 transconjugants were identified through selective plating. Screening for pTi15955 curing and loss of the pAt15955 segment was performed using loss of *gusA* or *lacZ* activity on 5-bromo-4-chloro-3-indolyl-β-glucuronic acid (X-Gluc) or 5-bromo-4-chloro-3-indolyl-β-D-galactopyranoside (X-Gal) as well as gentamicin or spectinomycin

sensitivity, respectively, and/or a combination of Eckhardt gel electrophoresis (Eckhardt 1978) and PCR. Eckhardt gel electrophoresis was performed according to a modified protocol (Personal communication, J. Griffitts, Brigham Young University, Provo, UT). Additionally, the presence of pTi15955 was also evaluated using octopine auxotrophy screening.

Ti plasmid reintroduction and conjugation assays

pTi15955::*gusA/*Gm^R was reintroduced into Sp^R *A. tumefaciens* 15955 backgrounds (IB128/IB129) through conjugation with IB123 (At+Ti+::*gusA*/Gm^R) as a donor in ATGN media supplemented with octopine [3.25 mM]. Briefly, donor and recipients were grown in ATGN supplemented with appropriate antibiotics to OD_{600} 0.6 and 100 µL of donor and recipient were combined and spotted onto sterile 0.2 µm cellulose acetate filter discs placed on ATGN media supplemented with octopine (ATGNO [3.25 mM]). After incubation (18 h, 28°C), the spots were resuspended in ATGN and plated onto ATGN supplemented with antibiotics to select for transconjugants. Transconjugants were confirmed using Eckhardt gel electrophoresis and PCR.

Conjugation assays were performed as described previously (Heckel et al. 2014) with alterations. Briefly, donors and recipient were grown and normalized to OD_{600} 0.6, mixed 1:1, and 100 µL was spotted onto 0.2 µm cellulose acetate filter discs placed on ATGN supplemented with and without octopine [3.25 mM]. Following incubation (18h, 28°C), matings were suspended in liquid ATGN, serially diluted, and spotted onto media supplemented with appropriate antibiotics. Conjugation efficiency was determined as the ratio of transconjugants per output donor.

Truncation of pAt15955 segment using Cre-lox

The *loxP* site (5' GCGGTCGAC<u>ATAACTTCGTATA</u>*ATGTATGC*<u>TATACGAAGTTAT</u>CATATGGCG 3', 18 bp inverted sequences are underlined, and the 8bp spacer is italicized) was introduced into four

locations within pAt15955::*lacZ*/Sp^R of IB118 in a pair-wise fashion to truncate either half of, or the entire pAt15955 segment upon transient expression of the Cre recombinase. To allow Cre-mediated deletion the left half of the At plasmid segment (denoted L), *loxP* sites were introduced in a tandem, direct orientation into positions L and CL that are interior to the flanking IS66 element and *lacZ*Sp^R marker in IB118, respectively, to create IB118 *lox*L (Figure S5 and Table S1). Deletion of right half (denoted R) of the segment was done similarly, except *loxP* sites were integrated at positions CR and R to create IB118 *lox*R. *loxP* sites were integrated at positions L and R to create IB118 *lox*L+R and allow deletion of the entire segment. Confirmation of genomic integration of each *loxP* site was done using PCR with primers specific for each integration site. Transient expression of the Cre recombinase was accomplished through introduction of the pCRE1-Ap suicide vector (Bailey et al. 2002) into the appropriate *A. tumefaciens* 15955 recipient (IB118 *lox*L, IB118 *lox*R, or IB118 *lox*L+R) via mating with *E.coli* S17-1/λpir pCRE1-Ap as described [1] with minor alterations. After mating of donor and recipients on LB agar, resuspensions were plated onto LB with or without Sp supplementation for deletion of the left and right half or entire segment, respectively. Confirmation of Cre-mediated deletions were confirmed using Eckhardt gel electrophoresis and PCR with primers specific for each new junction site created through Cre-mediated deletion.

Competition experiments

Competition experiments were performed as described previously with minor alterations (Morton et al. 2013). Competitor strains were grown in ATGN with or without antibiotic to an OD600nm of 0.6-0.8, washed 3 times in dd$H_2$0, and mixed 1:1 at an OD600nm of 0.01 in 2 mL of media. When competitions reached an OD600 nm of 0.6-0.8, 0.4-0.6, or 0.2-0.4 for replete carbon, limiting carbon, and virulence-inducing media, respectively, the competitions were serially diluted and spotted onto ATGN with and without antibiotic to enumerate each competitor, as well as sub-cultured (1:100) into the same media. Competitions were carried out for a total of

nine passages and each was performed 3 times with reciprocally-marked strains for a total of 6 replicates. Relative fitness was estimated as the number of doublings by each competitor over each passage during the course of the experiment, as described previously (Lenski 1988, Morton et al. 2013). Passaging intervals, such as P0-P9, thusly denote cumulative doublings over every passage.

RESULTS

Large deletion in pAt15955 upon pTi15955 curing.

Several on-going studies rely on curing of the Ti plasmid from *A. tumefaciens*, using a plasmid incompatibility, eviction process (Platt et al. 2012, Uraji et al. 2002, Yamamoto et al. 2018). As a matter of practice, the plasmid profiles of putatively cured derivatives are analyzed by Eckhardt gel electrophoresis to visualize their large plasmid content (see Materials and Methods). Eckhardt gel analysis of *A. tumefaciens* 15955 revealed two discrete bands, reflecting the presence of both an At plasmid (pAt15955, large band) and Ti plasmid (pTi15955, smaller band) (Figure 1). Several derivatives of *A. tumefaciens* 15955 were cured of their Ti plasmid using the incompatibility-eviction approach. Strikingly, it was observed that these cured derivatives of *A. tumefaciens* 15955 lost the Ti plasmid, but also lost the pAt band, replaced by a plasmid species that migrated faster than pAt but more slowly than pTi (Figure 1). This change in plasmid profile was observed for virtually all of the Ti plasmid-cured derivatives from multiple experiments, and suggested that the pAt plasmid had incurred a large deletion coincident with loss of the Ti plasmid. Interestingly, Eckhardt gel analysis of *A. tumefaciens* SA122, a 15955 derivative cured by a completely different approach using chemical and temperature stress in a different laboratory years earlier revealed the same pattern as the derivatives we had generated (Figure 1, and see Materials and Methods) (Uraji 2002, Yamamoto et al. 2018).

To confirm loss of pTi15955, as well as diagnose other genomic changes in these strains underlying the changes observed using Eckhardt gel electrophoresis, whole genome sequencing was conducted on WT *A. tumefaciens* 15955 and pTi15955-cured derivatives. WT *A. tumefaciens* 15955 assembled into 13 scaffolds, the first four corresponding to the circular chromosome (scaffold00001, 2.836 Mbp), linear chromosome (scaffold 00002, 2.082 Mbp), pAt (scaffold00003, 0.816 Mbp), and pTi (scaffold00004, 0.192 Mbp). Nine other smaller scaffolds did not assemble with the four primary scaffolds and ranged in size from 16.045 Kbp (scaffold00005) to 2.419 Kbp (scaffold00013). The sequencing readily confirmed loss of pTi15955 in cured derivatives but also identified a large (270,949 bp) deletion in the pAt15955 (Figure 2) that was consistent between multiple pTi15955-cured isolates (Figure 2 and data not shown). From this, we concluded the single band present in pTi15955-cured isolates upon Eckhardt gel electrophoresis is the truncated pAt15955 (denoted as pAt15955Δ270) (Figure 1). The *A. tumefaciens* 15955 genome sequence recently deposited in GenBank database (Bioproject PRJNA494475) does not have this deletion, and matches our de novo generated wild type sequence.

Evaluation of curing and deletion frequencies suggests these processes are linked but independent.

We have observed two separate, large scale genomic events, Ti plasmid curing and the large deletion incurred in pAt15955, occurring coincidentally. To characterize the connection between these events, the correlation between pTi15955 curing and pAt15955 segment loss was determined under pTi15955 curing conditions. Incompatibility-based curing strategies were used to correlate both events due to the high frequency of curing using this method (Uraji 2002, Yamamoto et al. 2018). Using this strategy, a broad host range plasmid (pBBR origin) containing a copy of the pTi15955 replication origin (*repABC*), a selectable kanamycin resistance marker (Km^R), and a counterselectable marker (*sacB*) is introduced into *A.*

tumefaciens 15955 strains via conjugal transfer from an *E. coli* donor and the resulting transconjuants that exhibit appropriate antibiotic resistance were screened for the loss of the Ti plasmid. Ti plasmids generally have a low copy number under standard laboratory conditions (Pappas 2008, Platt et al. 2014, Suzuki et al. 2001). Consequently, the presence of an additional copy of the Ti plasmid replication origin on a higher copy number plasmid can prevent proper maintenance and segregation of the Ti plasmid and lead to itsloss. The pTi15955 curing vector used here is similar to those described previously (Platt et al. 2012, Uraji 2002, Yamamoto et al. 2018) and detailed in the Materials and Methods.

To increase the efficiency by which both curing of pTi15955 and loss of the pAt15955 segment could be diagnosed, screenable and selectable marker cassettes were introduced into the *A. tumefaciens* 15955 genome within the pAt15955 segment (pos. 364,474) and on pTi15955 (pos. 17,447) using recombinational mutagenesis strategies described previously (Morton et al. 2012). A *lacZ*/Sp^R cassette and a *gusA*/Gm^R cassette were introduced between convergently oriented genes within the pAt15955 deletion segment and on pTi15955, respectively, to create IB118. Upon introduction of the curing plasmid, frequencies for loss of the pAt15955 segment and pTi15955 curing were determined through a combination of blue/white screening on X-Gal (β-galactosidase, LacZ indicator) or X-Gluc (β-glucuronidase, GusA indicator), followed by confirmation with Sp^S or Gm^S screening, respectively, and confirmed PCR and Eckhardt gel analysis. Loss of LacZ or GusA activity and Sp or Gm sensitivity in these reporter strains faithfully reported on pAt15955 segment loss or pTi15955 curing, respectively (data not shown).

Using the *A. tumefaciens* 15955-IB118 derivative with the *lacZ*/Sp^R and a *gusA*/Gm^R cassettes, it was determined that ~20% of curing plasmid transconjugants have lost pTi15955 under assay conditions (Table 1). Consistent with previous analyses of pTi15955-cured isolates (Figure 1), ~100% of pTi15955-cured isolates also incur loss of the pAt15955Δ270 segment (Table 1). However, ~71% of curing plasmid transconjugants incur loss of the segment, indicating that it is

deleted at a higher frequency than loss of the pTi15955 plasmid under these conditions (Table 1). Taken together, the correlation suggests that curing conditions stimulate pTi15955 curing and pAt15955 segment loss, that the events are separable, and that loss of the pAt15955 may precede, and/or possibly even limit, pTi15955 curing.

The frequencies observed above are consistent with a model in which a canonical toxin/anti-toxin (TA) module is separated between the pTi and pAt replicons, where an unlinked toxin on the pAt15955 segment and an anti-toxin on pTi15955 accounts for the observation that pAt15955 segment loss precedes pTi15955 curing. Although sequence searches using TAfinder (http://202.120.12.133/TAfinder/index.php) were able to identify putative TA systems on both pAt15955 and pTi15955 (Table S4), no separable, unlinked TA systems were identified using these programs. In general, a variety of genetic interactions between the pAt15955 segment and pTi15955 could function as TA systems, including cross-regulation of costly genes. For example, genomic stability may be undermined following pAt15955Δ270 deletion if this results in loss of regulatory repression of a costly factor encoded by pTi15955. These types of genetic interactions would be difficult to identify via bioinformatic analysis and may depend on undetermined environmental conditions. Interestingly, plasmid stabilization genes identified on pAt15955 were enriched outside of the deletion interval (Table S4), which may partially explain the propensity to lose this particular segment.

We also explored whether more general stress conditions could induce the observed pAt15955 deletion. Multiple individual isolates of *A. tumefaciens* 15955 isolates grown under standard conditions, antibiotic exposure, heat shock (37°C), and virulence-inducing conditions (acidic pH and plant phenolics) were examined for the deletion. None of the isolates tested (~3.0×10^8) had incurred the deletion suggesting that it is specifically induced by the curing process, although independent of the exact curing mechanism. This observation suggested that the loss

is specific to conditions which directly compromise replication of pTi15955 and may represent a genetic and functional link between both replicons (Table 1 and data not shown).

A. tumefaciens Ach5, an octopine-type strain that lacks the deleted pAt segment.

Strains belonging to the *A. tumefaciens* species complex have been classified based on their genome sequences into several genomospecies (Mougel et al. 2002), and *A. tumefaciens* 15955 falls into the G1 genomospecies (Henkel et al. 2014, Huang et al. 2015). *A. tumefaciens* Ach5 is another G1 genomospecies with an octopine-type Ti plasmid. Analysis of the Ach5 genome sequence (GenBank Access. No. Bioproject PRJNA278497) reveals that is missing the exact same large segment as we have observed to delete in 15955 under Ti plasmid curing conditions, with nearly identical sequence flanking this region (Figure S1) (Henkel et al. 2014, Huang et al. 2015). This suggests that the genomic lability of this segment has been manifested during the evolutionary history of Ach5, and that the propensity for the deletion event may be conserved within this subgroup of *A. tumefaciens* isolates.

The pAt15955 deletion event is mediated by flanking IS66 elements.

Analysis of whole genome sequencing data identified three copies of an IS element, IS66, within the *A. tumefaciens* 15955 genome, one on the linear chromosome (pos. 28,096-30652) and two on pAt15955 (IS66_At_L, pos. 508,310-510,865 and IS66_At_R, pos. 237,361-239,916), flanking the deletion interval (Figure S2). IS66 represents a family of IS elements conserved within a wide variety of bacteria, but was first identified on an octopine-type Ti plasmid within *A. tumefaciens* (Gourbeyre et al. 2010, Han et al. 2001, Machida et al. 1984). The element consists of three open reading frames, *tnpABC*, the latter of which is thought to encode an active transposase and is the most conserved across the IS66-family. The three ORFs are bordered by distinct direct and indirect repeats (Figure S2).

Repetitive sequences, such as IS-elements, are notoriously difficult to correctly assemble in next generation sequencing data. We aimed to confirm and enumerate the IS66 elements within *A. tumefaciens* 15955 and its deletion derivative using a Southern blot approach (in our de novo sequencing, prior to the deposit of the curated 15955 genome sequence, the number of IS66 copies was uncertain). A 515 bp DNA fragment specific for *tnpC* was generated by PCR (primers IBP102 and IBP103) and used to probe restriction enzyme-digested genomic DNA (*Sph*I, *Eco*RI, and *Bam*HI) from *A. tumefaciens* 15955 and its derivatives. In WT *A. tumefaciens* 15955 gDNA, three distinct bands were present in restriction digests, confirming that *A. tumefaciens* 15955 contains three copies of IS66 (Figure 3A). Fragment sizes of detected bands are consistent with two IS66 elements flanking the pAt15955 segment (Figure 3D). Strikingly, only two visible bands are detectable for gDNA from the IBE13A derivative, deleted for the At15955Δ270 plasmid segment, indicating loss of one IS66 element during the deletion event (Figure 3B). One of the two fragments matches a fragment in the wild type, and the second for the *Sph*I and *Eco*RI digests does not match either of the other two restriction fragments in the wild type. The *Bam*HI digest of the deletion mutant generates a predicted new fragment very close in size to the previous two. These observations are consistent with loss of one IS66 element and retention of a single copy of IS66 on pAt15955 at the site of deletion, and correlates with predictions from our own sequence analysis (Figure 3D) and examination of the GenBank 15955 accession.

While nearly all *A. tumefaciens* 15955 curing plasmid transconjugants that lose pTi15955 also lose the pAt15955 segment, we have recovered several rare isolates that have been cured of pTi15955 but do not carry the deletion, including derivative IBJUN138. Southern analysis of IBJUN138 did not deviate from the pattern observed for *A. tumefaciens* 15955 (Figure 3C), confirming our sequence assemblies suggesting that IS66 does not reside on the Ti plasmid in

this strain and rather is on the linear chromosome, in contrast to previous reports for IS66 on octopine-type Ti plasmids in other *A. tumefaciens* strains (Machida et al. 1984).

Retention of a single IS66 element following the deletion event suggests homologous recombination as the primary mechanism for segment deletion. Recombination-mediated deletion of the pAt15955 segment would require that both elements be in the same orientation (Petes et al. 1988). An inverse PCR approach was used to confirm that both IS66 elements flanking the pAt15955 segment in WT *A. tumefaciens* 15955 exist in a tandem orientation (Figure S4A). Based on predicted restriction fragment sizes surrounding each IS66 element in WT *A. tumefaciens* 15955, inverse PCR products support the direct orientation of both elements (Figure S4B and data not shown), also in agreement with the sequence assemblies.

As repetitive IS-elements are common substrates for homologous recombination, it seemed likely that the two IS66 elements on pAt15955 were responsible for the observed deletion during pTi15955 curing. To examine the role for both IS66 elements in mediating the pAt15955Δ270 deletion, the left copy of the IS66 element (IS66-At-L) was deleted from pAt15955 within the reporter strain IB118. The resulting strain (IB118ΔIS66) was subjected to pTi15955-curing conditions and evaluated for pAt15955 segment loss and pTi15955 curing. The pAt15955Δ270 deletion event in IB118ΔIS66 under pTi15955 curing conditions was undetectable (Table 1), consistent with the requirement for the two elements to drive homologous recombination. Interestingly, *A. tumefaciens* Ach5 also has a single copy of IS66 at the deletion site in pAtAch5, suggesting that IS66 may have mediated a similar large deletion in this strain (Figure S3). Insertion of many transposable elements creates a short duplication at the site of insertion, and this is reported to be 8 bp for IS66 (Machida et al. 1984). Unique 8 bp duplications flank all three of the IS66 elements in the 15955 sequence (IS66_Lin, AGAACACG; IS66_At_L, CCTTGATC;

IS66_At_R, CGTTCCGG). In contrast, for the pAt15955Δ270 deletion derivative the 8 bp sequences immediately flanking the left and right ends in the single remaining At plasmid IS66 element match the outside flanking sequence from the IS66_At_L and IS66_At_R, respectively (Fig. Sx). Similarly, the 8 bp flanking each end of IS66 in pAtAch5 are different from each other (CCGGAACG and CCTTGATC) and match those flanking the IS66 pAt15955Δ270. These observations are again consistent with homologous recombination between IS66 elements driving the deletion events in both the ancestor of pAtAch5 and in pAt15955.

The pAt15955 segment has a modest but detectable stabilizing effect on pTi15955

Our observations suggest a step-wise mechanism in which loss of the pAt15955 segment usually precedes pTi15955-curing (Table 1). However, we were able to obtain a rare derivative in which the Ti plasmid was cured, but the pAt15955 plasmid did not have the Δ270 deletion (IBJUN138). It seemed plausible that this derivative had incurred mutations which abolished the mechanism by which loss of the Ti plasmid stimulates the deletion event. However, whole genome sequence analysis of IBJUN138, did not reveal mutations within the deleted segment and none that would readily explain retention of this pAt segment (data not shown). We therefore used the IBJUN138 strain that had retained the intact At plasmid but was cured for the Ti plasmid, to examine the impact of the retained At plasmid genes on curing frequencies. The *gusA*/Gm^R-marked pTi15955 plasmid was reintroduced by conjugation back into two pTi15955-cured derivatives with a chromosomal Sp^R marker, one that had incurred loss of the pAt15955 segment (IB129) and another that had not (IB130, a derivative of IBJUN138) (Table S1 and Methods). These strains were then subjected to pTi15955-curing conditions and evaluated for Ti plasmid loss. The reintroduction strain, IB130, appeared to have a significant decrease in pTi15955 curing relative to other strains, and the IB129 strain that had already incurred the pAt15955 deletion was modestly elevated in pTi curing frequency (Table 1). These findings suggested that the presence of the pAt deletion segment may stabilize the Ti plasmid.

We sought to determine whether the Ti plasmid stabilization was due to a specific genetic locus within the deleted segment or tied to the carriage cost of this entire region. To test this question, the derivative carrying the marker in the deleted segment (IB118) was truncated for 138.8 kb on the left side (IB118 ∆L, pos. 504,337-365,531) or 106.7kb on the right side (IB118 ∆R, pos. 354,236-247,489) portion of the deleted segment, or the entire (IB118 ∆L+R) segment, using a Cre/*lox*-driven deletion approach (Figure S5, Table S1, and Methods). Strains truncated with Cre/*lox* retain both flanking IS66 copies and retain the *lacZ*Sp^R markers within the deletion interval, except for IB118∆L+R, in which the *lacZ*Sp^R markers are deleted but flanking IS66 elements are still retained (Figure S5). These engineered deletion derivatives were subjected to pTi15955-curing conditions, and evaluated for pTi15955-curing frequencies. Truncation of part, or the entire pAt15955 segment had modest, but measurable effects on pTi15955 stability (Table 1). The two derivatives deleted for either the entire element or its right half exhibited a modest increase in pTi15955 curing frequency, whereas the deletion of the left half of this segment was very similar to the wild type frequency (Table 1). This suggests that genetic elements within the right half of the pAt15955 segment may influence pTi15955 stability (Table 1). Similar Ti plasmid curing frequencies were observed for the isolated derivative deleted for the pAt15955 segment (IB129) with the single IS66 element and the engineered derivative lacking the genes on the segment, but retaining the tandem IS66 elements (IB118 ∆L+R), suggesting that the tandem IS66 elements alone do not influence pTi15955 stability (Table 1).

The modest alterations in pTi15955 stability in backgrounds with differing pAt15955 segment architectures suggests that the mechanism driving pAt15955 segment loss may be influenced by the genetic content within the deleted segment (likely via genetic elements in the right half of this segment), but this difference is unlikely to account for the tight correlation between the pAt deletion event and Ti plasmid curing we have observed.

pAt15955Δ270 segment contains conjugation machinery and conjugation of pAt15955 is octopine-inducible

Analysis of whole genome sequence data from WT *A. tumefaciens* 15955 identified conjugal transfer genes within pAt15955 that are homologous to functions on pTi15955 (Figure S6 and data not shown). Interestingly, unlike pTi15955 and other Ti plasmids, pAt15955 *trb* and *traI* are not directly divergent from *repABC* and are rather encoded within the AtΔ270 deletion segment (Figure S6). Thus, strains deleted for the pAt15955 segment are lacking *trb* and *traI* genes, which are essential for conjugation in Ti plasmids with similar systems (Li et al. 1998, Li et al. 1999), and so they may be incapable of conjugation. To test this, WT *A. tumefaciens* 15955 and derivatives that lack the pAt15955 segment, pTi15955, or both, were marked with Km^R and used in conjugation assays with the ERM52 recipient, a plasmidless (At^-Ti^-) *A. tumefaciens* C58 derivative marked with Sp^R (Figure 4, Methods). In standard growth conditions (ATGN), low level At plasmid conjugation was observed for the marked wild type (IB125), and this is abolished in the deleted derivative (AtΔ270 Ti^+) lacking the pAt15955 *trb* genes (IB131). (Figure 4). Conjugation of the Ti plasmid in octopine-type *A. tumefaciens* strains is strictly regulated by the presence of octopine and a complex quorum sensing process (Fuqua et al. 1994, Gordon et al. 2014, Hwang et al. 1994, Piper et al. 1993). Addition of octopine stimulates conjugal transfer frequency by two orders of magnitude in the At^+Ti^+ donor (IB125). Surprisingly octopine also stimulated significant pAt15955 conjugation in the Ti^+AtΔ270 deletion strain (Figure 4). The Ti^- AtΔ270 derivative (IB132) did not detectably conjugate, and conjugation in the At^+Ti^- strain (IB133) was the same as the uninduced At^+ Ti^+, but was not stimulated by octopine addition. These findings suggest that the pAt15955 can drive its own low-level conjugation, dependent on conjugal transfer genes in the deleted segment (*trb* and *traI*). Octopine addition stimulates pAt15955 conjugation and this is dependent on the Ti plasmid, and can even overcome the absence of the pAt15955Δ270 segment.

One explanation for pTi15955-dependent, octopine-induced transfer of pAt15955Δ270 is cointegrate formation between pAt15955 and pTi15955 prior to Ti-driven conjugal transfer. To determine whether both plasmids were transferred during conjugation assays, pAt15955 transconjugants were screened for the presence of pTi15955 using octopine auxotrophy screening and Eckhardt gel electrophoresis (Figure 5 and Figure S7). As expected, donors possess pTi15955 and either pAt15955 (IB125) or pAt15955Δ270 (IB131), while the recipient (ERM52) is plasmidless (Figure 5). Transconjugants from either donor show a mix of plasmid profiles; some have both plasmids whereas others have only the pAt15955 or pAt15955Δ270 plasmids (Figure 5). The transconjugants without the Ti plasmid are unlikely to have arisen due to co-integrate formation, and for the pAt15955Δ270 plasmid the pTi15955-encoded conjugal machinery can compensate for the missing *trb* and *traI* genes. However, because the octopine-induced conjugation of pAt15955Δ270 appeared lower than pAt15955 (Figure 4), we tested whether the proportion of co-transfer of both plasmids was affected by the pAt15955 segment, and found that it does not impact the co-transfer frequency (Figure S7).

pAt15955Δ270 segment deletion has environment-dependent fitness consequences

To determine whether the pAt15955 segment imposes fitness consequences that may explain a propensity to lose the segment, competition experiments between isogenic strains that either carry or have lost the pAt15955 segment were performed under replete carbon, limiting carbon, and virulence-inducing conditions over nine serial passages (Figure 6). In replete carbon conditions, there was not a measurable fitness cost associated with the pAt15955Δ270 segment over the duration of the experiment. In limiting carbon conditions, there was a modest, measurable fitness effect of the segment that is similar to carriage costs determined for At plasmid deletions of a similar size in *A. tumefaciens* C58 (Morton et al. 2013). In the high-stress, virulence-inducing conditions, there was a significant fitness disadvantage to possessing the pAt15955 segment (Figure 6), suggesting that the presence of this region either increases

general susceptibility to the stressful conditions of virulence-induction or potentiates the *vir* response under these conditions, both of which could result in a decrease of growth-based fitness as measured in this assay.

DISCUSSION

Members of the family *Rhizobiaceae* exhibit signs of replicon co-evolution (Lassalle et al. 2017, Slater et al. 2009, Wang et al. 2018) and cross-replicon interactions (Barnett et al. 2004, Bobik et al. 2006, diCenzo et al. 2018, Galardini et al. 2015, Heidelberg et al. 2000, Pini et al. 2015, Ramachandran et al. 2017, Ronson et al. 1987), despite remarkable strain-to-strain variation and the prevalence of large-scale rearrangements in secondary replicons (Galardini et al. 2015, Lopez-Guerrero et al. 2012, Mazur et al. 2011, Morton et al. 2013, Orozco-Mosqueda Mdel et al. 2009). *A. tumefaciens* is a member of this family and often carries a large proportion of its genomic DNA, including important niche-associated functions, on two large extrachromosomal megaplasmids, pAt and pTi (Goodner et al. 2001, Wood et al. 2001). Given the prevalence of both Ti and At plasmids within *A. tumefaciens* isolates and bioinformatic evidence suggesting co-evolution of these replicons (Lassalle et al. 2017), cross-replicon interactions are likely to exist and in part function to co-stabilize the replicons. To this effect, we have previously shown evidence of co-stability of both replicons in *A. tumefaciens* C58 (Morton et al. 2014), suggesting favorable interactions between both plasmids in some strains.

Here, we show that curing of the Ti plasmid in the octopine-type strain *A. tumefaciens* 15955 drives a large deletion in the co-resident At plasmid, suggesting a discrete genetic link between both plasmids that may underlie co-replicon stability. Our observations suggested that the At plasmid was somehow limiting Ti curing. We hypothesized that the Ti plasmid was being stabilized, perhaps through a toxin-antitoxin-like interaction between both replicons, where a

toxin (or other costly function) on the At plasmid segment would be unchecked upon curing of the Ti plasmid. Bioinformatic searches were able to identify multiple putative TA systems on the At plasmid (Table S4), but none resided within the deletion segment and were actually enriched outside of the segment, a distribution that might possibly contribute to the dispensability of this region on pAt, but not explaining the propensity to lose the pAt15955Δ270 segment under curing conditions. However, we found that deletion of ~108 kb on the right half of this segment marginally increased pTi curing frequencies, suggesting that the genetic content in this region does impact overall Ti plasmid stability. The somewhat modest affect we observed provides evidence for cross-replicon stability between both plasmids, and this may be exacerbated in certain environmental conditions, but it seems unlikely that this observed stabilization explains the tight correlation between pTi curing and At plasmid segment loss that we report here.

The deletion event itself is mediated by a repetitive IS-element, IS66, that flanks the At segment and is required for its loss under curing conditions. IS66 was first identified on the Ti plasmid of a different octopine-type strain of *A. tumefaciens* (Machida et al. 1984) and is part of a larger family of IS-elements found within a variety of bacteria (Gourbeyre et al. 2010, Han et al. 2001). IS-elements are common vehicles for genome rearrangements and responsible for genome reduction in many bacterial taxa, including species of *Bordatella* (Parkhill et al. 2003, Siguier et al. 2006). Ti plasmid curing could conceivably elicit loss of the At plasmid segment through transposition of both flanking IS66 elements in a mechanism similar to a composite transposon (Bellanger et al. 2014). However the observed retention of a single element at the site after deletion with distint flanking duplications, and the tandem orientation of IS66 in full length pAt suggests homologous recombination as the mechanism for AtΔ270 segment loss, and hence should require RecA (Bell et al. 2016). Deletion of *recA* would clearly confirm whether homologous recombination is required for loss of the At plasmid segment. Whereas *recA* has been deleted previously in *A. tumefaciens* C58 (Farrand et al. 1989), our repeated attempts at

generating a similar deletion in *A. tumefaciens* 15955 were unsuccessful (suggesting that the mutation is deleterious in 15955).

The IS66-mediated deletion observed here is different from another set of At plasmid large deletions we have reported for *A. tumefaciens* C58, which appear to be mediated by small repeat sequences (Morton et al. 2013). The low degree of At plasmid synteny and the propensity of these plasmids to undergo large-scale rearrangements (Morton et al. 2013) suggests that the fitness benefit of gene content on the At plasmid may be highly environment-dependent. This is also true for the Ti plasmid, which imposes a heavy fitness burden upon exposure to virulence-inducing conditions (Platt et al. 2012), as well as other organisms, including species of *Methylobacterium*, where experimental evolution resulted in an environment-dependent reduction of the accessory genome by ~10% (Lee et al. 2012).

Genomic stability can be maintained in variety of ways, including the reduction of costs associated with accessory genes (diCenzo et al. 2017). For example, the stability of Ti plasmids is in part due to low carriage costs, low copy number, and extremely tight regulation of costly genes, including virulence functions and conjugal transfer (Morton et al. 2014, Pappas 2008, Pappas et al. 2003, Platt et al. 2012, Platt et al. 2012). The current results have important consequences for our previous estimates of the low carriage costs of the pTi15955 because these experiments unknowingly involved strains that had incurred the pAt1599Δ270 kb deletion (Platt et al. 2012). In our previous work, we concluded that under conditions which do not induce the Ti plasmid virulence genes and are not substantially expressed, there was a low but measurable carriage cost associated with pTi15955, while under virulence inducing conditions there was a large cost associated with pTi15955. The findings reported here show that the measurement of low, but significant basal carriage cost under non-inducing conditions reported in that paper is likely a combination of costs associated with the Ti plasmid and costs associated with the deleted At plasmid segment. The pAt15955Δ270 deletion alone results in a significant

fitness gain under similar experimental conditions (Figure 6) and thus the carriage cost of the Ti plasmid reported in the previous paper is likely to be less than estimated (Platt, Bever et al. 2012) and more similar to the low Ti plasmid carriage costs we determined for pTiC58 from the nopaline-type *A. tumefaciens* strain C58 (Morton et al. 2014).

The At plasmid deletion observed here had significant effects on overall fitness in an environment-dependent manner. While the segment conferred carriage costs similar to At plasmid deletions we have characterized previously (Morton et al. 2013), the burden of harboring the segment was significantly increased under virulence-inducing conditions. Virulence genes are induced by a combination of low phosphate and acidic pH, in addition to the presense of plant phenolics (Platt et al. 2012), so these conditions are also highly stressful and may exacerbate the fitness cost of harboring this large segment of the megaplasmid. However, the increased cost of this segment of pAt under virulence induction also may suggest a role for the At plasmid in the response of *A. tumefaciens* to the disease environment. This is consistent with our observations in *A. tumefaciens* C58, where the At plasmid was found to modulate virulence gene expression (Morton et al. 2013).

We identified additional interactions between these plasmids via their conjugal transfer functions. We observed that pAt15955 conjugation exhibits a basal level of conjugation that is further stimulated by the presence of octopine, the so-called conjugal opine for many octopine-type Ti plasmids (Klapwijk et al. 1978). The basal conjugation of pAt15955 in the absence of octopine is similar to that observed for the At plasmid of the nopaline-type *A. tumefaciens* strain C58, in which pAtC58 conjugates constitutively under laboratory conditions via its own conjugal transfer functions (Chen et al. 2002). The predicted pTiC58 conjugal pilus is encoded by the *avhB* genes (*Agrobacterium* virulence homologue *virB*), named as such due to their high homology to the pTiC58 plasmid-encoded VirB type IV secretion system which delivers T-DNA from *A. tumefaciens* to plants during infection. The *avhB* genes are more distantly similar to the

pTiC58 conjugal pilus (*trb)* genes. In contrast, the pAt15955 *trb* genes within the At∆270 segment we describe here are more closely similar to the pTi15955 conjugal transfer (*tra/trb*) genes then they are to *virB* genes on pTi15955. The basal conjugation of pAt15955 is not affected by the presence of the pTi15955 plasmid, whereas the presence of pTiC58 decreases pAtC58 conjugation by 10-fold (Chen et al. 2002). However, activation of the pTiC58 *tra* genes was reported to stimulate pAtC58 conjugal transfer (Lang et al. 2013). This was hypothesized to proceed through activation of the *rctB* regulator of pAtC58 conjugal transfer functions. Interestingly, our genome sequence reveals that pAt15955 has no *rctB*-type regulator and instead carries its own paralogues of the Ti plasmid quorum sensing control genes, *traR* and *traM* on the plasmid backbone, and the AHL synthese *traI* along with the *trb* genes, in the At∆270 segment. The TraR-TraI-TraM quorum sensing regulators on the Ti plasmid provide strict octopine and population density-dependent control of pTi conjugation for octopine-type Ti plasmids (Fuqua et al. 1995, Fuqua et al. 1996, Fuqua et al. 1994) and there is some evidence that in a close relative of 15955, the strain *A. tumefaciens* A6, these quorum sensing regulators may also regulate pAt conjugal transfer genes (Wang et al. 2014). The strong stimulation of pAt15955 by octopine, but only in the presence of the Ti plasmid, suggests that octopine may trigger these regulators to increase *tra* gene expression. Co-transfer of the At and Ti plasmid has been observed previously in the plant tumor environment (Lang et al. 2013), but we show here that it is directly related to octopine-induction of the Ti plasmid conjugation system and that both plasmid systems interact. Intriguingly, independent, octopine-inducible transfer of the pAt15955 plasmid that is missing the At∆270 segment which includes the *trb* and *traI* genes, only transfers in the presence of pTi15955, suggesting that it may also be able to co-opt the Ti *trb* functions for its own conjugation.

The genetic interaction between the At and Ti plasmids characterized here suggests extensive cross-replicon interactions between these replicons that may underlie their overall stability in

changing environments. As a large proportion of bacteria possess multiple large replicons, especially in *A. tumefaciens* and other members of *Rhizobiaceae*, similar interactions are likely to occur in those systems and may exert a profound influence on genomic stability. However, given the complex life histories associated with many of these bacteria, it will be challenging to identify the relevant environmental conditions which influence stability as well as the fitness costs associated with large-scale rearrangements.

ACKNOWLEDGEMENTS

This work was supported by National Institutes of Health Grant [R01 GM092660 to C.F. and J.D.B] and the Indiana Faculty Research Support Program (FRSP). We thank James D. Bever (JDB) for serving as PI on the R01 grant. We also thank Grace Perkins for technical assistance in the plasmid curing studies, Dean Rowe-Magnus for reagents and advice for engineering large deletions using the Cre-*lox* system, and the Center for Genomics and Bioinformatics at Indiana University for their work preparing the Illumina libraries and operating the sequencing instrumentation.

References

Agnoli, K et al. (2012). Exposing the third chromosome of *Burkholderia cepacia* complex strains as a virulence plasmid. Mol Microbiol 83(2): 362-378.

Bailey, J,Manoil, C (2002). Genome-wide internal tagging of bacterial exported proteins. Nat Biotechnol 20(8): 839-842.

Barnett, MJ, Toman, CJ, Fisher, RF,Long, SR (2004). A dual-genome Symbiosis Chip for coordinate study of signal exchange and development in a prokaryote–host interaction. Proc Natl Acad Sci, USA 101(47): 6.

Bell, JC,Kowalczykowski, SC (2016). RecA: Regulation and mechanism of a molecular search engine. Trends Biochem Sci 41(6): 491-507.

Bellanger, X, Payot, S, Leblond-Bourget, N,Guedon, G (2014). Conjugative and mobilizable genomic islands in bacteria: evolution and diversity. FEMS Microbiol Rev 38(4): 720-760.

Bobik, C, Meilhoc, E,Batut, J (2006). FixJ: a major regulator of the oxygen limitation response and late symbiotic functions of *Sinorhizobium meliloti*. J Bacteriol 188(13): 4890-4902.

Bolger, AM, Lohse, M,Usadel, B (2014). Trimmomatic: a flexible trimmer for Illumina sequence data. Bioinformatics 30(15): 2114-2120.

Carver, TJ et al. (2005). ACT: the Artemis Comparison Tool. Bioinformatics 21(16): 3422-3423.

Chain, PSG et al. (2006). *Burkholderia xenovorans* LB400 harbors amulti-replicon, 9.73-Mbp genome shaped for versatility. Proc Natl Acad Sci, USA 103(42): 8.

Chen, L, Chen, Y, Wood, DW,Nester, EW (2002). A new Type IV secretion system promotes conjugal transfer in *Agrobacterium tumefaciens*. Journal of Bacteriology 184(17): 4838-4845.

Deatherage, DE,Barrick, JE (2014). Identification of mutations in laboratory-evolved microbes from next-generation sequencing data using breseq. Methods Mol Biol 1151: 165-188.

diCenzo, GC,Finan, TM (2017). The divided bacterial genome: Structure, function, and evolution. Microbiol Mol Biol Rev 81(3).

diCenzo, GC et al. (2014). Examination of prokaryotic multipartite genome evolution through experimental genome reduction. PLoS Genet 10(10): e1004742.

diCenzo, GC, Wellappili, D, Golding, GB,Finan, TM (2018). Inter-replicon gene flow contributes to transcriptional integration in the *Sinorhizobium meliloti* multipartite genome. G3 (Bethesda) 8(5): 1711-1720.

Dougherty, K et al. (2014). Multiple phenotypic changes associated with large-scale horizontal gene transfer. PLoS One 9(7): e102170.

Eckhardt, T (1978). A rapid method for the identification of plasmid desoxyribonucleic acid in bacteria. Plasmid 1: 584-588.

Escobar, MA,Dandekar, AM (2003). *Agrobacterium tumefaciens* as an agent of disease. Trends Plant Sci. 8(8): 380-386.

Farrand, SK, O'Morchoe, SP,McCutchan, J (1989). Construction of an *Agrobacterium tumefaciens* C58 *recA* mutant. J Bacteriol 171(10): 8.

Finan, TM, Kunkel, B, De Vos, GF,Signer, ER (1986). Second symbiotic megaplasmid in *Rhizobium meliloti* carrying exopolysaccharide and thiamine synthesis genes. J Bacteriol 167(1): 7.

Funnell, BE,Phillips, GJ (2004). Plasmid Biology. Washington, D.C., ASM Press.

Fuqua, C, Burbea, M,Winans, SC (1995). Activity of the *Agrobacterium* Ti plasmid conjugal transfer regulator TraR is inhibited by the product of the *traM* gene. J Bacteriol 177(5): 7.

Fuqua, C,Winans, SC (1996). Conserved *cis*-acting promoter elements are required for density-dependent transcription of *Agrobacterium tumefaciens* conjugal transfer genes. J Bacteriol 178(2): 6.

Fuqua, WC,Weiner, RM (1993). The *melA* gene is essential for melanin biosynthesis in the marine bacterium *Shewanella colwelliana*. J Gen Microbiol. 139(5): 10.
Fuqua, WC,Winans, SC (1994). A LuxR-LuxI type regulatory system activates *Agrobacterium* Ti plasmid conjugal transfer in the presence of a plant tumor metabolite. J Bacteriol 176(10): 11.
Galardini, M et al. (2015). Evolution of intra-specific regulatory networks in a multipartite bacterial genome. PLoS Comput Biol 11(9): e1004478.
Galardini, M et al. (2013). Replicon-dependent bacterial genome evolution: the case of *Sinorhizobium meliloti*. Genome Biol Evol 5(3): 542-558.
González, M et al. (2005). The partitioned *Rhizobium etli* genome: Genetic and metabolic redundancy in seven interacting replicons. Proc Natl Acad Sci, USA 103(10): 6.
Goodner, B et al. (2001). Genome sequence of the plant pathogen and biotechnology agent *Agrobacterium tumefaciens* C58. Science 294(5550): 2323-2328.
Gordon, JE,Christie, PJ (2014). The *Agrobacterium* Ti plasmids. Microbiol Spectr 2(6).
Gourbeyre, E, Siguier, P,Chandler, M (2010). Route 66: Investigations into the organisation and distribution of the IS66 family of prokaryotic insertion sequences. Res Microbiol 161(2): 136-143.
Han, CG et al. (2001). Structural and functional characterization of IS679 and IS66-family elements. J Bacteriol 183(14): 4296-4304.
Heckel, BC et al. (2014). *Agrobacterium tumefaciens exoR* controls acid response genes and impacts exopolysaccharide synthesis, horizontal gene transfer, and virulence gene expression. J Bacteriol 196(18): 3221-3233.
Heidelberg, JF et al. (2000). DNA sequence of both chromosomes of the cholera pathogen *Vibrio cholera*e. Nature 406: 8.
Henkel, CV, den Dulk-Ras, A, Zhang, X,Hooykaas, PJ (2014). Genome sequence of the Octopine-type *Agrobacterium tumefaciens* strain Ach5. Genome Announc 2(2).
Huang, Y-Y et al. (2015). Complete Genome Sequence of *Agrobacterium tumefaciens* Ach5. Genome Announc 3(3): 2.
Hwang, I et al. (1994). TraI, a LuxI homologue, is responsible for production of conjugation factor, the Ti plasmid *N*-acylhomoserine lactone autoinducer. Proc Natl Acad Sci, USA 91: 5.
Klapwijk, PM, Scheulderman, T,Schilperoort, RA (1978). Coordinated regulation of octopine degradation and conjugative transfer of Ti plasmids in *Agrobacterium tumefaciens*: Evidence for a common regulatory gene and separate operons. J Bacteriol 136(2): 11.
Kurtz, S et al. (2004). Versatile and open software for comparing large genomes. Genome Biol. 5(2): 9.
Lang, J et al. (2013). Concerted transfer of the virulence Ti plasmid and companion At plasmid in the *Agrobacterium tumefaciens*-induced plant tumour. Mol Microbiol.
Langmead, B,Salzberg, SL (2012). Fast gapped-read alignment with Bowtie 2. Nat Methods 9(4): 357-359.
Lassalle, F et al. (2017). Ancestral genome estimation reveals the history of ecological diversification in *Agrobacterium*. Genome Biol Evol 9(12): 3413-3431.
Lee, MC,Marx, CJ (2012). Repeated, selection-driven genome reduction of accessory genes in experimental populations. PLoS Genet 8(5): e1002651.
Lenski, R (1988). Experimental studies of pleiotropy and epistasis in *Escherichia coli*. I. Variation in competitive fitness among mutants resistant to virus T4. Evolution 42(3): 8.
Li, P-L, Everhart, DM,Farrand, SK (1998). Genetic and sequence analysis of the pTiC58 trb locus, encoding a mating-pair formation system related to members of the Type IV secretion family. J Bacteriol 180(23): 9.
Li, P-L, Hwang, I, Miyagi, H,Farrand, SK (1999). Essential components of the Ti plasmid *trb* system, a Type IV macromolecular transporter. J Bacteriol 181(16): 9.

Lopez-Guerrero, MG et al. (2012). Rhizobial extrachromosomal replicon variability, stability and expression in natural niches. Plasmid 68(3): 149-158.
Machida, Y et al. (1984). Nucleotide sequence of the insertion sequence found in the T-DNA region of mutant Ti plasmid pTiA66 and distribution of its homologues in octopine Ti plasmid. Proc Natl Acad Sci, U S A 81: 5.
Mauchline, TH et al. (2014). Mapping the *Sinorhizobium meliloti* 1021 solutebinding protein-dependent transportome. Proc Natl Acad Sci, USA 103(47): 6.
Mazur, A et al. (2011). Intragenomic diversity of *Rhizobium leguniosarum* bv. trifolii clover nodule isolates. BMC Microbiol 11: 123.
Morton, ER,Fuqua, C (2012). Genetic manipulation of *Agrobacterium*. Curr Protoc Microbiol: Unit 3D 2.
Morton, ER,Fuqua, C (2012). Laboratory maintenance of *Agrobacterium*. Curr Protoc Microbiol: Unit3D 1.
Morton, ER, Merritt, PM, Bever, JD,Fuqua, C (2013). Large deletions in the pAtC58 megaplasmid of *Agrobacterium tumefaciens* can confer reduced carriage cost and increased expression of virulence genes. Genome Biol Evol 5(7): 1353-1364.
Morton, ER, Platt, TG, Fuqua, C,Bever, JD (2014). Non-additive costs and interactions alter the competitive dynamics of co-occurring ecologically distinct plasmids. Proc Biol Sci 281(1779): 20132173.
Mougel, C, Thioulouse, J, Perrière, G,Nesme, X (2002). A mathematical method for determining genome divergence and species delineation using AFLP. Int. J. Syst. Evol. Microbiol. 52: 14.
Orozco-Mosqueda Mdel, C et al. (2009). Homologous recombination and dynamics of rhizobial genomes. Res Microbiol 160(10): 733-741.
Pappas, KM (2008). Cell-cell signaling and the *Agrobacterium tumefaciens* Ti plasmid copy number fluctuations. Plasmid 60(2): 89-107.
Pappas, KM,Winans, SC (2003). A LuxR-type regulator from *Agrobacterium tumefaciens* elevates Ti plasmid copy number by activating transcription of plasmid replication genes. Mol Microbiol 48(4): 15.
Parkhill, J et al. (2003). Comparative analysis of the genome sequences of *Bordetella pertussis*, *Bordetella parapertussis* and *Bordetella bronchiseptica*. Nat Genet 35(1): 32-40.
Petes, TD,Hill, CW (1988). Recombination between repeated genes in microorganisms. Annu Rev Genet 22: 22.
Pini, F et al. (2015). Cell cycle control by the master regulator CtrA in *Sinorhizobium meliloti*. PLoS Genet 11(5): e1005232.
Piper, KR, Beck von Bodman, S,Farrand, SK (1993). Conjugation factor of *Agrobacterium tumefaciens* regulates Ti plasmid transfer by autoinduction. Nature 362(1): 3.
Platt, TG, Bever, JD,Fuqua, C (2012). A cooperative virulence plasmid imposes a high fitness cost under conditions that induce pathogenesis. Proc Biol Sci 279(1734): 1691-1699.
Platt, TG, Fuqua, C,Bever, JD (2012). Resource and competitive dynamics shape the benefits of public goods cooperation in a plant pathogen. Evolution 66(6): 1953-1965.
Platt, TG et al. (2014). Ecological dynamics and complex interactions of *Agrobacterium* megaplasmids. Front Plant Sci 5: 635.
Ramachandran, R, Jha, J, Paulsson, J,Chattoraj, D (2017). Random versus cell cycle-regulated replication initiation in bacteria: insights from studying *Vibrio cholerae* chromosome 2. Microbiol Mol Biol Rev 81(1).
Romanchuk, A et al. (2014). Bigger is not always better: Transmission and fitness burden of ∼1 MB *Pseudomonas syringae* megaplasmid pMPPla107. Plasmid 73: 10.
Ronson, CW, Nixon, BT, Albricht, LM,Ausubel, FM (1987). *Rhizobium meliloti ntrA* (*rpoN*) gene is required for diverse metabolic functions. J Bacteriol 169(6): 8.

Siguier, P, Filee, J,Chandler, M (2006). Insertion sequences in prokaryotic genomes. Curr Opin Microbiol 9(5): 526-531.
Slater, SC et al. (2009). Genome sequences of three agrobacterium biovars help elucidate the evolution of multichromosome genomes in bacteria. J Bacteriol 191(8): 2501-2511.
Suzuki, K, Iwata, K,Yoshida, K (2001). Genome analysis of *Agrobacterium tumefaciens*: construction of physical maps for linear and circular chromosomal dnas, determination of copy number ratio and mapping of chromosomal virulence genes. DNA *Res* 8: 12.
Uraji, M, Suzuki, K,Yoshida, K (2002). A novel plasmid curing method using incompatibility of plant pathogenic Ti plasmids in *Agrobacterium tumefaciens*. Genes Genet. Syst. 77: 1-9.
Uraji, M, Suzuki, K., and Yoshida, K. (2002). A novel plasmid curing method using incompatibility of plant pathogenic Ti plasmids in *Agrobacterium tumefaciens*. Genes Genet. Syst. 77: 1-9.
Van Larebeke, N et al. (1974). Large plasmid in *Agrobacterium tumefaciens* essential for crown gall-inducing ability. Nature 252: 10.
Wang, C, Yan, C, Fuqua, C,Zhang, LH (2014). Identification and characterization of a second quorum-sensing system in *Agrobacterium tumefaciens* A6. J Bacteriol 196(7): 1403-1411.
Wang, X et al. (2018). Comparative analysis of rhizobial chromosomes and plasmids to estimate their evolutionary relationships. Plasmid 96-97: 13-24.
Watson, B et al. (1975). Plasmid required for virulence of *Agrobacterium tumefaciens*. J Bacteriol 123: 10.
Wood, DW et al. (2001). The Genome of the Natural Genetic Engineer *Agrobacterium tumefaciens* C58. Science 294: 8.
Xie, Y et al. (2018). TADB 2.0: an updated database of bacterial type II toxin-antitoxin loci. Nucleic Acids Res 46(D1): D749-D753.
Yamamoto, S et al. (2018). Effective removal of a range of Ti/Ri plasmids using a pBBR1-type vector having a repABC operon and a lux reporter system. Appl Microbiol Biotechnol 102(4): 1823-1836.

Table 1: pAt15955 segment deletion and pTi15955 curing frequencies under incompatibility-based pTi15955 curing conditions.

Strain	Genotype		Ti curing conditions	
	pAT	pTi	At deletion freq.[a]	Ti curing freq.[b]
WT (IB118/IB126)[c]	+	+	0.71 ± 0.10	0.28 ± 0.08
IB118 ΔIS66	+	+	< 3.0 x 10^{-8}	Not determined
IB129	Δ270	+ (RI)[d]	NA	0.45 ± 0.17
IB130	+	+ (RI)[d]	Not determined	0.13 ± 0.08
IB118 ΔL	Δ130 L	+	Not determined	0.27 ± 0.04
IB118 ΔR	Δ130 R	+	Not determined	0.42 ± 0.17
IB118 ΔL+R	Δ270	+	NA	0.39 ± 0.07

[a]At deletion frequency determined as the ratio of *A. tumefaciens* curing plasmid transconjugants that have incurred the At plasmid deletion to total transconjugants.

[b]Ti curing frequency determined as the ratio of *A. tumefaciens* curing plasmid transconjugants that have lost the Ti plasmid to total transconjugants. ~100% of isolates cured for pTi15955 have also incurred the pAt15955Δ270 deletion and only rare isolates have been recovered that retain the segment upon pTi15955 curing (text and Table S1).

[c]WT represents combined data from IB118 and IB126 for At deletion and Ti curing frequencies.

[d]RI – indicates that pTi15955 was re-introduced by conjugation

FIGURE LEGENDS

Figure 1: Multiple changes in plasmid profile of *A. tumefaciens* 15955 upon curing of pTi15955. Eckhardt gel electrophoresis analysis of WT *A. tumefaciens* 15955 and two derivatives of *A. tumefaciens* 15955, cured of the Ti plasmid (pTi15955) using either chemical (SA122) or plasmid incompatibility methods (IB124). Positions of pAt15955 and pTi15955 in WT *A. tumefaciens* 15955 are shown. Arrow indicates single band present in pTi15955-cured derivatives.

Figure 2: Whole genome sequencing confirms co-incident pAt15955 deletion upon pTi15955 curing. Mummerplot visualization of MUMmer 3 alignment of genome assembly scaffolds from WT 15955 (X axis) and a pTi15955-cured derivative (IB124, Y axis) confirm loss of a large, ~270 Kbp segment in pAt15955 upon pTi15955 curing. Matching sequence between assemblies is indicated with diagonal red line segments. Sequence corresponding to each replicon is indicated. Inset (dashed) highlights large (270 Kbp) deletion of pAt15955 and absence of pTi15955 in IB124.

Figure 3: Loss of one IS66 element upon deletion of ~270 Kbp pAt15955 segment. Southern blot analysis of gDNA from WT *A. tumefaciens* 15955 (**A**) and two derivatives that have either incurred loss of the pAt15955 segment (IBE13A, **B**) or pTi15955 (IBJUN138, **C**) using three restriction enzyme digests that do not cleave within IS66 (SphI, EcoRI, and BamHI). Ladder shown is NEB 1 kb DNA ladder. Numbers on Y-axis indicated ladder sizes in Kbp. **D)** Bioinformatic prediction of IS66-containing restriction fragment sizes for digests in A, B, and C – color coding matches the dots adjacent to each band. In A and C, two hybridizing fragments correspond to IS66 elements flanking pAt15955 segment and one to IS66 on the linear

chromosome. In B, one hybridizing fragment corresponds to the linear chromosome and one to the remaining fragment to IS66 on pAt15955Δ270 at deletion site.

Figure 4: Octopine-inducible pAt15955 conjugation is pTi15955-dependent and independent of pAt15955-encoded *trb* machinery. pAt15955 conjugation frequencies of marked (Km^R) derivatives of *A. tumefaciens* 15955 into a plasmidless recipient, ERM52, under standard growth (ATGN, dark gray) and octopine-containing (ATGNO, hatched, 3.25 mM) conditions. Strains shown are WT (IB125) or derivatives deleted for pAt15955 segment (IB131), pTi15955 (IB133), or both (IB132). Conjugation frequencies reported as transconjugants per output donor (Methods). A and B denote p-value <0.03.

Figure 5: Co-transfer of pTi15955 in pAt15955 transconjugants in the presence of octopine. Plasmid profiles for subset of pAt15955 transconjugants from conjugation assay in Figure 4 were determined by Eckhardt gel electrophoresis. Shown are profiles for two donors (IB125 and IB131), recipient (ERM52), and three transconjugants from conjugation assays with either donor (IB125 or IB131). Indicated below gel image are presence (+) or absence (-) of pTi15955 and the presence of WT pAt15955 (+) or pAt15955Δ270 (Δ270).

Figure 6: pAt15955 segment loss confers an environment-dependent fitness advantage. Relative fitness of WT *A. tumefaciens* 15955 and a strain isogenic for loss of the pAt15955 segment over one (P0-P1), five (P0-P5) and nine (P0-P9) serial passages in replete carbon (dark gray), limiting carbon (hatched), and virulence-inducing conditions (white). Bars represent 6 biological replicates, 3 each with inversely marked strains (Methods). Relative fitness calculated as the total number of doublings of each competitor over the indicated passing

interval (Methods). Error bars shown are standard deviation. Asterisk indicates p-value < 0.05 in comparison to the expectation of 1.

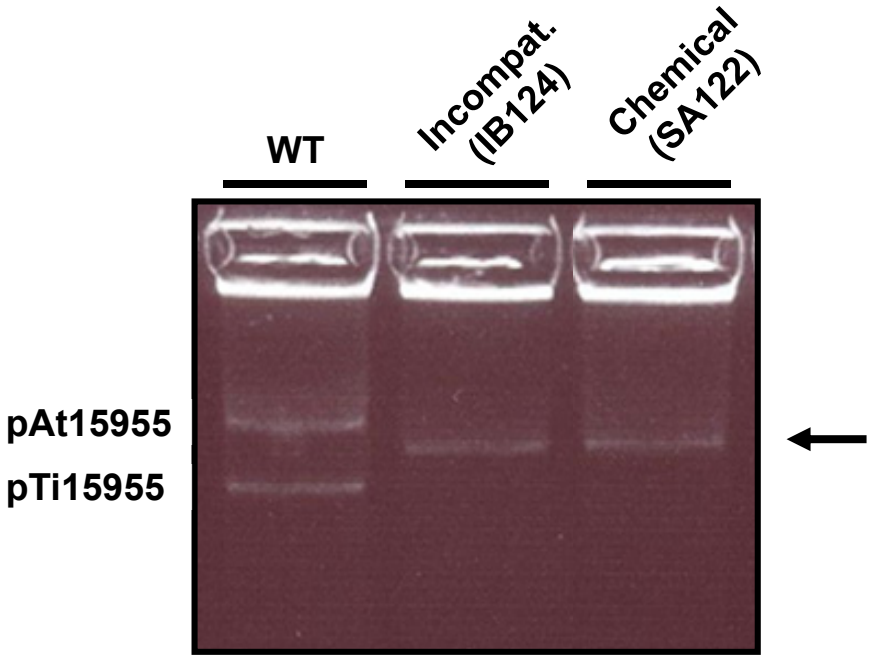

Figure 1: Multiple changes in plasmid profile of *A. tumefaciens* 15955 upon curing of pTi15955. Eckhardt gel electrophoresis analysis of WT *A. tumefaciens* 15955 and two derivatives of *A. tumefaciens* 15955, cured of the Ti plasmid (pTi15955) using either chemical (SA122) or plasmid incompatibility methods (IB124). Positions of pAt15955 and pTi15955 in WT *A. tumefaciens* 15955 are shown. Arrow indicates single band present in pTi15955-cured derivatives.

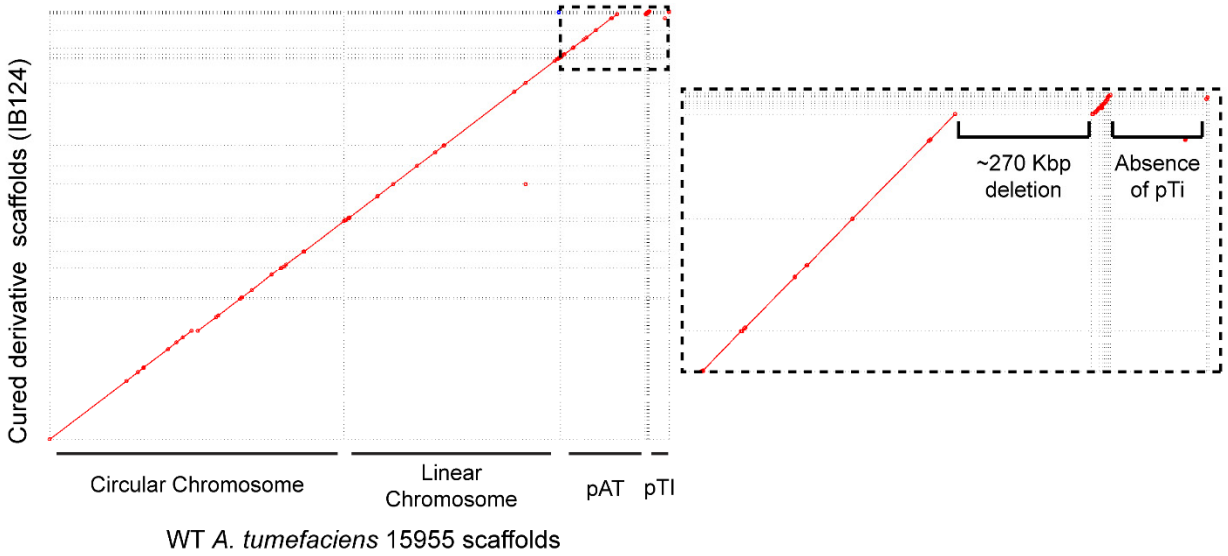

Figure 2: Whole genome sequencing confirms co-incident pAt15955 deletion upon pTi15955 curing. Mummerplot visualization of MUMmer 3 alignment of genome assembly scaffolds from WT 15955 (X axis) and a pTi15955-cured derivative (IB124, Y axis) confirm loss of a large, ~270 Kbp segment in pAt15955 upon pTi15955 curing. Matching sequence between assemblies is indicated with diagonal red line segments. Sequence corresponding to each replicon is indicated. Inset (dashed) highlights large (270 Kbp) deletion of pAt15955 and absence of pTi15955 in IB124.

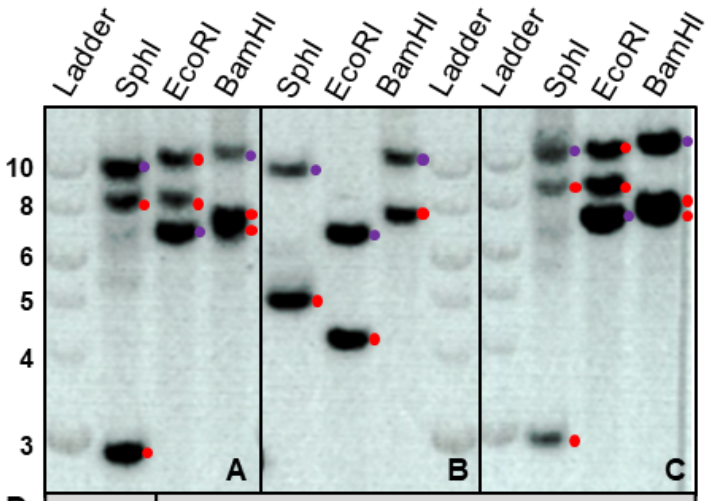

D

Panel	Predicted fragment sizes (Kbp)		
	SphI	EcoRI	BamHI
A	9.9, 8.1, 2.8	10.3, 8.2, 6.6	10.3, 6.8, 7.2
B	9.9, 4.9	6.6, 4.1	10.3, 7.3
C	9.9, 8.1, 2.8	10.3, 8.2, 6.6	10.3, 6.8, 7.2

Figure 3: Loss of one IS66 element upon deletion of ~270 Kbp pAt15955 segment. Southern blot analysis of gDNA from WT *A. tumefaciens* 15955 (**A**) and two derivatives that have either incurred loss of the pAt15955 segment (IBE13A, **B**) or pTi15955 (IBJUN138, **C**) using three restriction enzyme digests that do not cleave within IS66 (SphI, EcoRI, and BamHI). Ladder shown is NEB 1 kb DNA ladder. Numbers on Y-axis indicated ladder sizes in Kbp. **D)** Bioinformatic prediction of IS66-containing restriction fragment sizes for digests in A, B, and C – color coding matches the dots adjacent to each band. In A and C, two hybridizing fragments correspond to IS66 elements flanking pAt15955 segment and one to IS66 on the linear chromosome. In B, one hybridizing fragment corresponds to the linear chromosome and one to the remaining fragment to IS66 on pAt15955Δ270 at deletion site.

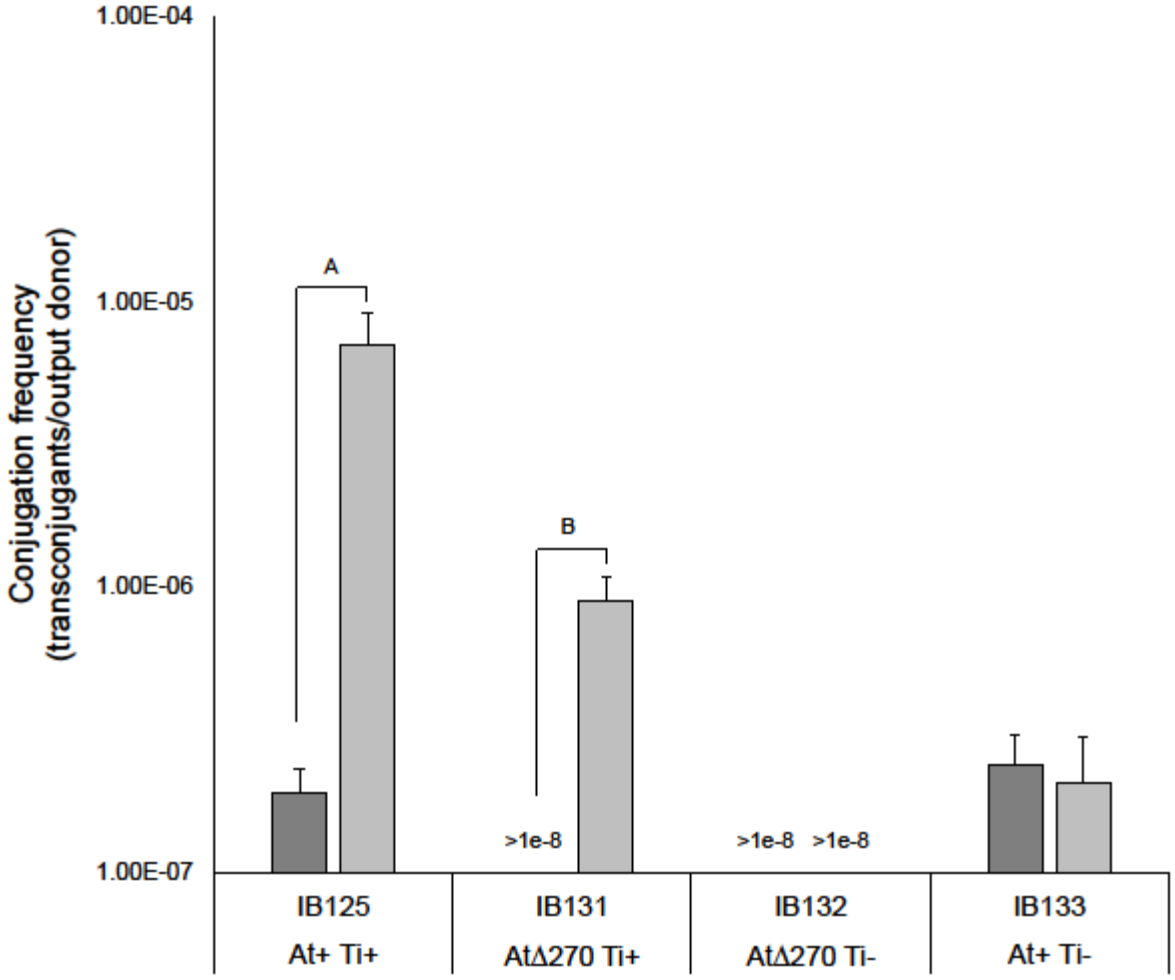

Figure 4: Octopine-inducible pAt15955 conjugation is pTi15955-dependent and independent of pAt15955-encoded *trb* machinery. pAt15955 conjugation frequencies of marked (Km^R) derivatives of *A. tumefaciens* 15955 into a plasmidless recipient, ERM52, under standard growth (ATGN, dark gray) and octopine-containing (ATGNO, hatched, 3.25 mM) conditions. Strains shown are WT (IB125) or derivatives deleted for pAt15955 segment (IB131), pTi15955 (IB133), or both (IB132). Conjugation frequencies reported as transconjugants per output donor (Methods). A and B denote p-value <0.03.

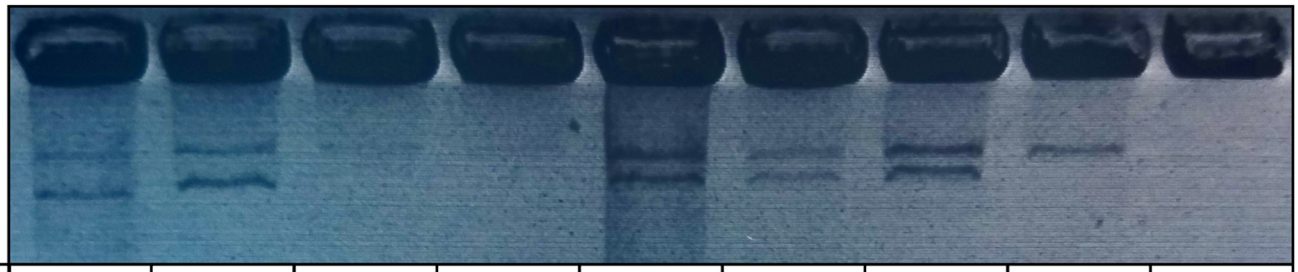

	Donor (IB125)	Transconjugants (IB125)			Donor (IB131)	Transconjugants (IB131)			Recip. (ERM52)
pAt	+	+	+	+	Δ270	Δ270	Δ270	Δ270	-
pTi	+	+	-	-	+	+	+	-	-

Figure 5: Co-transfer of pTi15955 in pAt15955 transconjugants in the presence of octopine. Plasmid profiles for subset of pAt15955 transconjugants from conjugation assay in Figure 4 were determined by Eckhardt gel electrophoresis. Shown are profiles for two donors (IB125 and IB131), recipient (ERM52), and three transconjugants from conjugation assays with either donor (IB125 or IB131). Indicated below gel image are presence (+) or absence (-) of pTi15955 and the presence of WT pAt15955 (+) or pAt15955Δ270 (Δ270).

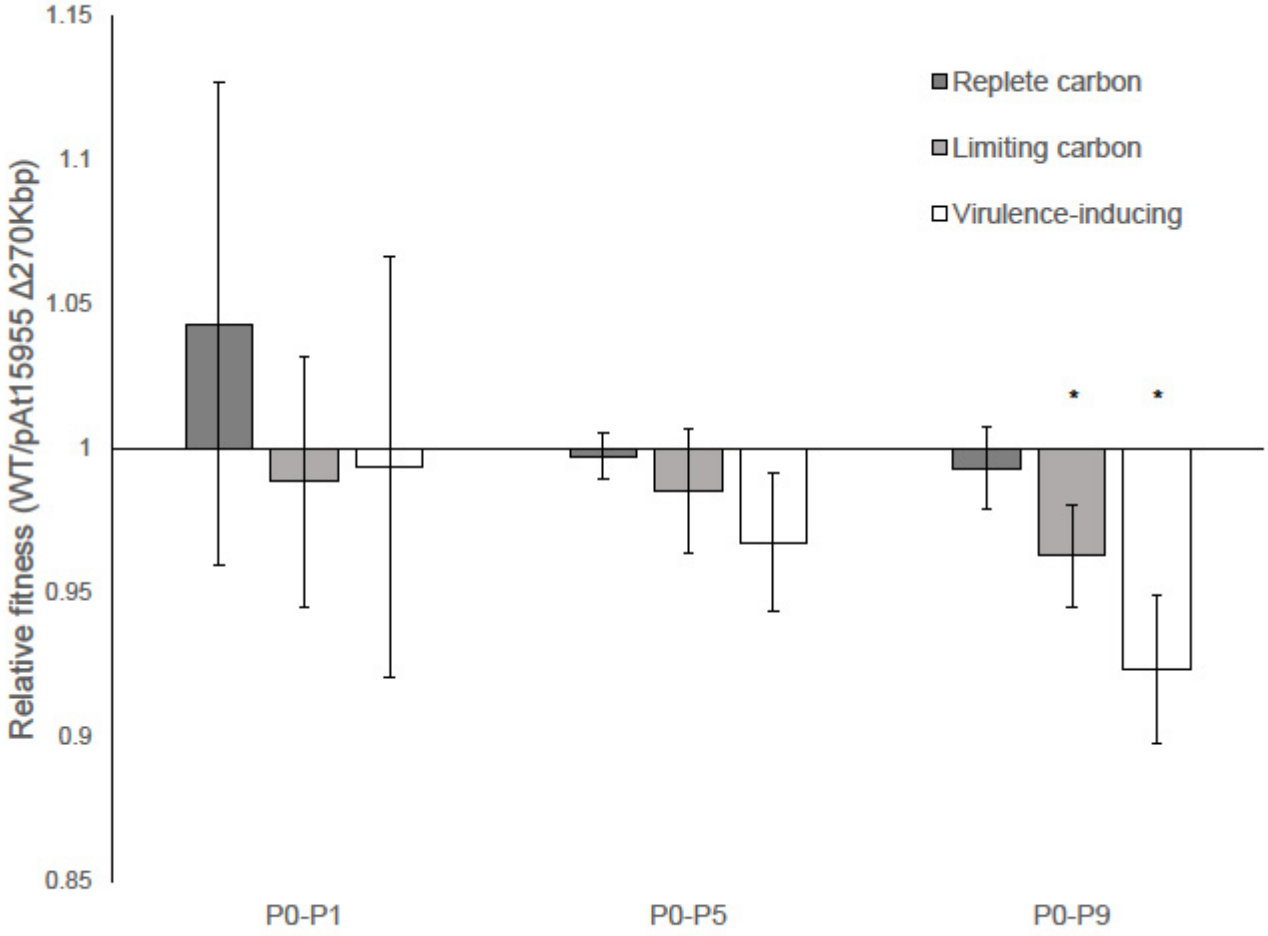

Figure 6: pAt15955 segment loss confers an environment-dependent fitness advantage. Relative fitness of WT *A. tumefaciens* 15955 and a strain isogenic for loss of the pAt15955 segment over one (P0-P1), five (P0-P5) and nine (P0-P9) serial passages in replete carbon (dark gray), limiting carbon (hatched), and virulence-inducing conditions (white). Bars represent 6 biological replicates, 3 each with inversely marked strains (Methods). Relative fitness calculated as the total number of doublings of each competitor over the indicated passing interval (Methods). Error bars shown are standard deviation. Asterisk indicates p-value < 0.05 in comparison to the expectation of 1.